Structural Chirality of Polar Skyrmions Probed by Resonant Elastic X-Ray Scattering

Margaret R. McCarter,[1,*] Kook Tae Kim,[2,*] Vladimir A. Stoica,[3,4] Sujit Das,[5] Christoph Klewe,[6] Elizabeth P. Donoway,[1] David M. Burn,[7] Padraic Shafer,[6] Fanny Rodolakis,[3] Mauro A. P. Gonçalves,[8] Fernando Gómez-Ortiz,[9] Jorge Íñiguez,[10,11] Pablo García-Fernández,[9] Javier Junquera,[9] Stephen W. Lovesey,[7,12] Gerrit van der Laan,[7] Se Young Park,[2] John W. Freeland,[3] Lane W. Martin,[13,14] Dong Ryeol Lee,[2,†] and Ramamoorthy Ramesh[1,13,14,‡]

[1]*Department of Physics, University of California, Berkeley, California 94720, USA*
[2]*Department of Physics, Soongsil University, Seoul 06978, Korea*
[3]*Advanced Photon Source, Argonne National Laboratory, Lemont, Illinois 60439, USA*
[4]*Department of Materials Science and Engineering, Pennsylvania State University, Pennsylvania 16802, USA*
[5]*Materials Research Centre, Indian Institute of Science, Bangalore 560012, India*
[6]*Advanced Light Source, Lawrence Berkeley National Laboratory, Berkeley, California 94720, USA*
[7]*Diamond Light Source, Harwell Science and Innovation Campus, Didcot, Oxfordshire OX11 0DE, United Kingdom*
[8]*Institute of Physics of the Czech Academy of Sciences, 18221 Prague 8, Czech Republic*
[9]*Departmento de Ciencias de la Tierra y Física de la Materia Condensada, Universidad de Cantabria, 39005 Santander, Spain*
[10]*Materials Research and Technology Department, Luxembourg Institute of Science and Technology (LIST), 5 avenue des Hauts-Fourneaux, L-4362 Esch/Alzette, Luxemburg*
[11]*Department of Physics and Materials Science, University of Luxembourg, Rue du Brill 41, L-4422 Belvaux, Luxembourg*
[12]*Department of Physics, Oxford University, Oxford OX1 3PU, United Kingdom*
[13]*Department of Materials Science and Engineering, University of California, Berkeley, California 94720, USA*
[14]*Materials Sciences Division, Lawrence Berkeley National Laboratory, Berkeley, California 94720, USA*

(Received 12 November 2021; revised 8 March 2022; accepted 23 October 2022; published 5 December 2022)

An escalating challenge in condensed-matter research is the characterization of emergent order-parameter nanostructures such as ferroelectric and ferromagnetic skyrmions. Their small length scales coupled with complex, three-dimensional polarization or spin structures makes them demanding to trace out fully. Resonant elastic x-ray scattering (REXS) has emerged as a technique to study chirality in spin textures such as skyrmions and domain walls. It has, however, been used to a considerably lesser extent to study analogous features in ferroelectrics. Here, we present a framework for modeling REXS from an arbitrary arrangement of charge quadrupole moments, which can be applied to nanostructures in materials such as ferroelectrics. With this, we demonstrate how extended reciprocal space scans using REXS with circularly polarized x rays can probe the three-dimensional structure and chirality of polar skyrmions. Measurements, bolstered by quantitative scattering calculations, show that polar skyrmions of mixed chirality coexist, and that REXS allows valuation of relative fractions of right- and left-handed skyrmions. Our quantitative analysis of the structure and chirality of polar skyrmions highlights the capability of REXS for establishing complex topological structures toward future application exploits.

DOI: 10.1103/PhysRevLett.129.247601

Nontrivial order-parameter topologies in ferroelectrics and ferromagnets provide a playground to study nanoscale interactions, topological protection, and their potential use in next-generation applications [1]. Particularly, in ferroelectrics, configurations of interest include skyrmions [2], vortices [3], and hopfions [4], all of which have curling dipolar textures. While such magnetic features have been studied for at least a decade [5,6], polar analogs were not experimentally confirmed until recently [7,8] despite being theoretically predicted in the early 2000s [9–11]. Whereas magnetic skyrmions typically range in size from tens to hundreds of nanometers, polar skyrmions are less than ten nanometers in size.

As sizes decrease, the potential for novel functionalities of these features grows, but their nondestructive characterization also becomes increasingly difficult. These structures are often chiral, which can affect their dynamics [2], so it is important to have characterization methods to determine not only structure, but also chirality. The challenge is to find a technique that can simultaneously probe chirality and three-dimensional (3D) polarization textures at very short length scales. To address this challenge, new techniques are called upon for resolving extended atomic arrangements beyond simple periodic orders.

Resonant elastic x-ray scattering (REXS) has emerged as an ideal technique to study such nanostructures, as it is an element- and orbital-specific probe that also provides

sensitivity to various electromagnetic multipoles in a material (i.e., the multipoles that comprise complex textures in ferroelectric and ferromagnetic materials) [12–16]. Selection of an ion type occurs by matching the incident x-ray energy with an atomic transition, with the benefit of accessing different orbitals. An additional strength of REXS is its ability to precisely determine spatially varying magnetic and orbital configurations [16–18]. Characterization of the magnetization vector distribution of chiral structures, such as domain walls and skyrmions, is a new frontier [19–24]. The successful REXS characterization of magnetic skyrmions depends on an already well-established framework that describes the interaction between polarized x rays and magnetic structures [12,13,25].

This technique can, in turn, be extended to studies of nonmagnetic chiral structures [26], and circular dichroism in REXS has been used to identify chirality in polar vortices [27] and skyrmions [8]. A minimal tensor model has shown that circular dichroism emerges in anisotropic tensor scattering from a one-dimensional, helical array of charge quadrupole moments [28,29], which is consistent with the helixlike winding of polarization in vortex and skyrmion structures.

Because of its sensitivity to ordered phases and ability to resolve spatially varying properties, REXS should also be able to provide detailed information on the 3D chiral structure of ferroelectric vortices and skyrmions in a way that is not accessible with other techniques. However, to gain this information, a generalized theoretical framework is needed. Here, we have developed a computational model of REXS from an ordered array of charge quadrupole moments. We demonstrate its utility by describing REXS experiments of polar skyrmions in a $PbTiO_3/SrTiO_3$ superlattice, which yields insights into their 3D structure and chirality.

Superlattices of $(PbTiO_3)_{16}(SrTiO_3)_{16}$ (PTO/STO) were grown epitaxially on STO (001) substrates using pulsed laser deposition (for details see Supplemental Material [30] and Ref. [8]). The ferroelectric polarization in the PTO layers forms polar skyrmion structures as illustrated in Fig. 1(a), which has been experimentally demonstrated and confirmed by second-principles simulations [8]. Each skyrmion has an out-of-plane polarization at its center (which defines the skyrmion polarity $P = \pm 1$), surrounded by a matrix of the opposite polarization [see Fig. 1(b)]. The in-plane polarization winds continuously either counterclockwise (CCW) or clockwise (CW), which defines the helicity ($H = \pm 1$) of the skyrmion [see Fig. 1(c)]. This curling pattern makes the skyrmions chiral and distinguishes these structures from typical 180° ferroelectric domains. The chirality of a skyrmion is determined by its polarity and helicity, and it is defined as $C = P \cdot H$, with $C = +1$ or -1 defining a right- or left-handed skyrmion [33]. Two $P = -1$ skyrmions with opposite chirality are shown in Figs. 1(b) and 1(c).

The polar skyrmions form a quasiordered ensemble, which aligns preferentially along the in-plane x and y directions. Nonresonant, hard x-ray diffraction reciprocal space maps were initially used to characterize the ordered polar phase via the complex strain field that is generated. In a typical reciprocal space map [see Fig. 2(a)], there are superlattice peaks along the crystal truncation rod (the out-of-plane Q_z direction), as well as lateral satellite peaks (along the in-plane Q_{lateral} direction) due to the skyrmion lattice.

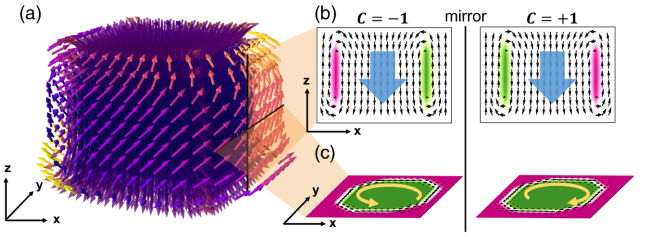

FIG. 1. Polar skyrmion structure. (a) 3D skyrmion structure adapted from second-principles calculations, with arrows representing dipoles from the ferroelectric polarization. (b) Two-dimensional polarization maps of the xz plane for skyrmions with the same polarity ($P = -1$) but opposite chirality. The black arrows represent the polarization direction. The green (magenta) [light gray (dark gray)] coloring represents polarization pointing into (out of) the page. The two skyrmions are mirror images. (c) Two-dimensional polarization maps of the xy plane with yellow (white) arrows showing the rotation of in-plane polarization at the skyrmion domain wall. The green (magenta) [light gray (dark gray)] coloring represents polarization along the negative (positive) z direction.

In ferroelectric PTO, Ti^{4+} cations are displaced along the polarization direction in each unit cell of the parent tetragonal structure. The chiral polarization texture of the skyrmions should, in turn, lead to a chiral arrangement of the titanium orbitals. Considering this, REXS with circularly polarized light at the titanium $L_{2,3}$ edge (457 eV) was measured. This edge corresponds to electronic transitions from the spin-orbit split $2p_{1/2}$ (L_2) and $2p_{3/2}$ (L_3) orbitals to the unoccupied $3d$ orbitals (which are split into the t_{2g} and e_g orbitals, based on symmetry).

Spectra measured at $Q_{\text{lateral}} = 0.73$ nm^{-1} (corresponding to the 8.6 nm spacing of the polar skyrmions) and $Q_z = 1.5$ nm^{-1} (corresponding to the third-order diffraction peak from the superlattice periodicity of 12 nm) show that REXS from polar skyrmions exhibits strong x-ray circular dichroism (XCD) [the difference in scattered intensity for right- (RCP) or left-circularly polarized (LCP) x rays] due to their chiral structure, as seen in Fig. 2(b). Additionally, the circular dichroism switches sign upon reversal of the sign of the lateral scattering vector ($Q_{\text{lateral}} = \pm 0.73$ nm^{-1}) as shown in Fig. 2(c), which is an indication of chirality in magnetic systems [21,22].

Previous studies of polar vortices and skyrmions have focused on circular dichroism measurements at a single pair of scattering vectors at $\pm Q_{\text{lateral}}$ to prove that the polar nanostructures are chiral [8,27]. Here, we use extended reciprocal space scans combined with detailed calculations to model the 3D structure of the skyrmions.

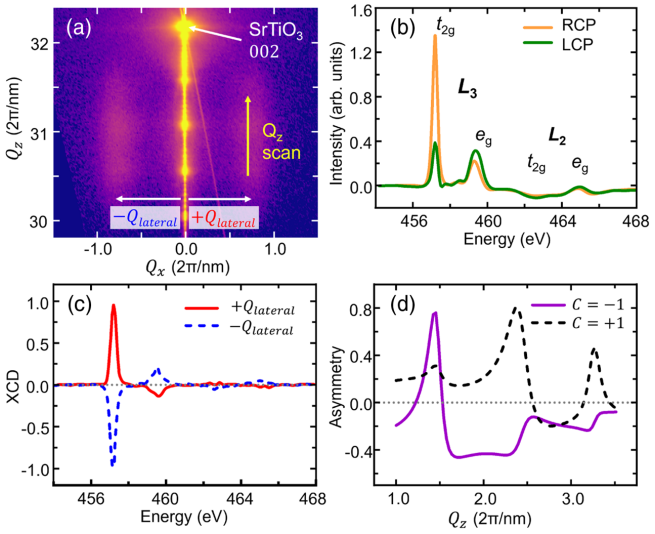

FIG. 2. Nonresonant x-ray diffraction and REXS. (a) Nonresonant x-ray diffraction (Thomson scattering) is sensitive to periodic structural distortions, giving rise to lateral satellite peaks from the polar skyrmion ordering at $Q_{\mathrm{lateral}} = \pm 0.73\ \mathrm{nm}^{-1}$. The vertical yellow (white) arrow represents where the Q_z rod scan is measured. (b) Intensity of resonant x-ray scattering with RCP and LCP x rays measured at $Q_{\mathrm{lateral}} = 0.73\ \mathrm{nm}^{-1}$ and $Q_z = 1.5\ \mathrm{nm}^{-1}$. (c) X-ray circular dichroism at $\pm Q_{\mathrm{lateral}}$. (d) Calculated asymmetry ratios for a Q_z rod scan at a fixed energy and $Q_{\mathrm{lateral}} = +0.73\ \mathrm{nm}^{-1}$ for left- and right-handed skyrmions (chirality $C = \mp 1$).

In general, x-ray scattering measured at different points in reciprocal space will probe ordering in different crystallographic directions. When a crystal truncation rod scan is performed along the Q_z direction at the lateral satellite peak corresponding to the ordering of polar skyrmions [Q_z rod scan shown schematically in Fig. 2(a)], REXS should sensitively probe the 3D distribution of the electric polarization vectors constituting the chiral polar structure, because structural information is measured in both the in- and out-of-plane directions.

Based on this, we simulated the asymmetry ratio of a Q_z rod scan at the lateral satellite peak for an array of left- or right-handed skyrmions [see Fig. 2(d)]. The asymmetry ratio A is defined as

$$A = \frac{I_{\mathrm{RCP}} - I_{\mathrm{LCP}}}{I_{\mathrm{RCP}} + I_{\mathrm{LCP}}}, \tag{1}$$

where I_{RCP} and I_{LCP} are the diffracted intensity for incident RCP or LCP x rays. The asymmetry is unique for the left- versus right-handed skyrmions, showing that the chirality can be distinguished using this measurement. However, despite the fact that the left- and right-handed skyrmions are mirror images of one another, the asymmetry ratio is not exactly mirrored (antisymmetric) as one may initially

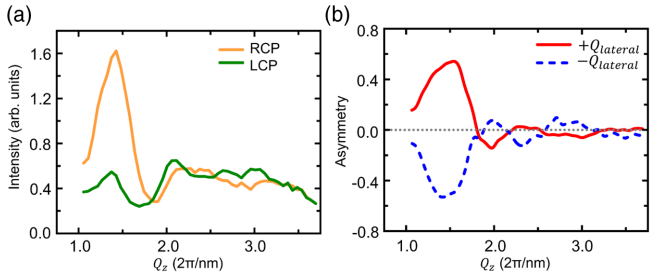

FIG. 3. Satellite crystal truncation rod scans. (a) Q_z rod scans at a fixed $Q_{\mathrm{lateral}} = +0.73\ \mathrm{nm}^{-1}$ measured with RCP and LCP x rays. (b) Circular dichroism asymmetry measured at $\pm Q_{\mathrm{lateral}}$.

guess, which further indicates the need for a deeper investigation to understand these results.

To explore this, Q_z rod scans of satellite peaks ($Q_{\mathrm{lateral}} = \pm 0.73\ \mathrm{nm}^{-1}$) were performed at constant energy (457.2 eV), for both RCP and LCP incident x rays. The result for $Q_{\mathrm{lateral}} = +0.73\ \mathrm{nm}^{-1}$ is shown in Fig. 3(a). We observe a strong dependence of the circular dichroism asymmetry on the scattering vector, as shown in Fig. 3(b). Interestingly, the asymmetry oscillates between positive and negative values as the out-of-plane scattering vector is varied. This means that, although the circular dichroism is indicative of chirality, the interpretation of the meaning of positive or negative circular dichroism [such as in the fixed-Q spectra in Fig. 2(c)] is not straightforward. Moreover, the superlattice periodicity and the period of oscillations in the asymmetry do not match, which points to the fact that the oscillations are solely due to the nature of the skyrmion chirality. To understand this strong variation of the asymmetry, we turn to detailed scattering calculations.

The REXS process is described by the resonant-scattering amplitude $f_{\epsilon'\epsilon}$. This describes the interaction of incident x rays with energy E, which are absorbed so that electrons transfer from the ground state labeled ϕ_ν of energy E_ν to the excited state ψ_η of energy E_η and relax again, emitting x rays of the same energy. In the dipole approximation, the resonant scattering amplitude can be described by the Kramers-Heisenberg dispersion formula [34,35]

$$f_{\epsilon'\epsilon} = \sum_\eta \frac{\langle \phi_\nu | \boldsymbol{\epsilon}' \cdot \boldsymbol{R} | \psi_\eta \rangle \langle \psi_\eta | \boldsymbol{\epsilon} \cdot \boldsymbol{R} | \phi_\nu \rangle}{E - (E_\eta - E_\nu) + i\Gamma}, \tag{2}$$

where $\boldsymbol{\epsilon}'$ and $\boldsymbol{\epsilon}$ are unit polarization vectors of the incident and scattered x rays, respectively, $\boldsymbol{R}$ is the electron position operator, and Γ is related to the characteristic lifetime of the excited state. It is well known that when the resonant atom is magnetic, the resonant scattering amplitude is usually expressed by the Hannon equation [36], which contains the magnetization vector $\boldsymbol{M}$.

However, the selection rules for electric-dipole transitions, which are the dominant transitions in the soft x-ray region, require that the multipole under study is parity even

[13,14]. This means that it is not permitted to replace $\boldsymbol{M}$ by an electric dipole moment $\boldsymbol{E}$, since $\boldsymbol{M}$ is time-odd and parity-even, whereas $\boldsymbol{E}$ is time-even and parity-odd. Instead, Lovesey and van der Laan [28] have shown that it is allowed to use the quadrupole moment of the excited state. In this case an ordered chiral arrangement of quadrupole moments of the excited state can give rise to circular dichroism in REXS.

The resonant scattering amplitude can be rewritten as

$$f_{\boldsymbol{\epsilon}'\boldsymbol{\epsilon}} = \boldsymbol{\epsilon}' \cdot \boldsymbol{T} \cdot \boldsymbol{\epsilon} = \sum_{ij} \epsilon'_i \epsilon_j T_{ij}, \tag{3}$$

where the anisotropic tensor (AT) $\boldsymbol{T}$ is introduced. This 3×3 matrix based on Cartesian coordinates encompasses different origins of resonant scattering, such as scattering from charge quadrupoles, which arise due to the crystalline anisotropy in materials such as ferroelectrics. This form of scattering is also called anisotropic x-ray anomalous scattering or Templeton-Templeton scattering [37–40].

In the case of a single crystal, resonant ions at different sites inside the unit cell have different ATs due to crystal field or hybridization from surrounding ions. In the case of the polar skyrmions generated in PTO/STO superlattices, the changing ferroelectric polarization in each unit cell means that the AT also varies. It can be shown through quantitative electronic structure calculations of the AT that unit cells with varying polarization can be simply related to the AT of Ti^{4+} in the tetragonal phase (see Supplemental Material [30] for details).

In addition to the changing AT, the resonant ion has a displacement vector $\boldsymbol{r}_n$ from the unit cell center that is proportional to the polarization vector. When calculating the structure factor for the unit supercell, the effect of the displacement vector on the phase factor for each resonant ion must also be considered. The structure factor $F_{\boldsymbol{\epsilon}'\boldsymbol{\epsilon}}$ of the repeating supercell of the polar skyrmion can be expressed as follows:

$$F_{\boldsymbol{\epsilon}'\boldsymbol{\epsilon}} = \boldsymbol{\epsilon}' \cdot \boldsymbol{\Psi} \cdot \boldsymbol{\epsilon}, \tag{4}$$

$$\boldsymbol{\Psi} = \frac{1}{N} \sum_{n=0}^{N-1} e^{i\vec{\boldsymbol{q}} \cdot (\vec{\boldsymbol{L}}_n + \vec{\boldsymbol{r}}_n)} \boldsymbol{T}_n, \tag{5}$$

where $\boldsymbol{T}_n$ is the AT of the resonant ion in the nth unit cell and $\vec{\boldsymbol{L}}_n$ is the translational vector pointing to the center of the nth unit cell (see Supplemental Material [30] for more details). In resonant scattering, the AT and x-ray polarization dependence make it possible to unambiguously determine information about the 3D distribution of polarization in the skyrmions. The detailed calculation method can be found in the Supplemental Material [30,41].

The asymmetry ratio of Q_z rod scans was quantitatively calculated from Eqs. (4), (S3), and (S4) using the polarization vector distribution of skyrmions obtained from second-principles calculations for skyrmions of different chiralities [see polarization maps in Fig. 1(b) and 1(c)]. The asymmetry ratio calculated for the satellite peaks $\pm Q_{\text{lateral}}$ [see Figs. 4(a) and 4(b) for skyrmions with chirality $C = -1$ and $+1$, respectively] shows no antisymmetric feature between the satellites of the opposite sign, unlike the experimental result. This is also different from the magnetic case where the circular dichroism is typically antisymmetric at two mirrored scattering vectors [19–23].

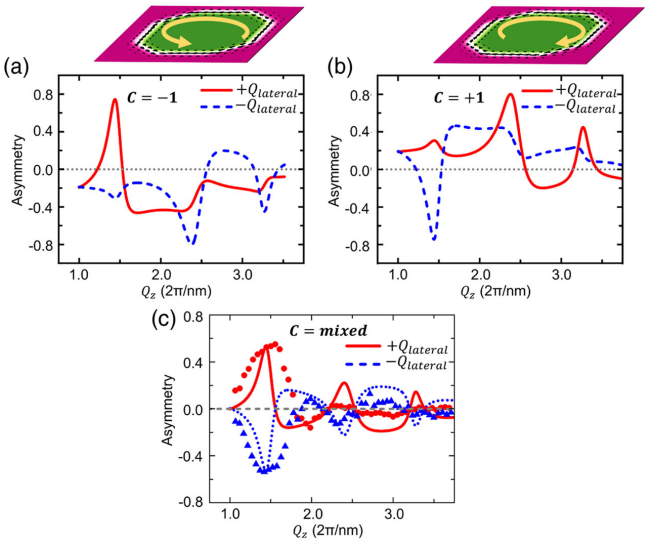

FIG. 4. Resonant x-ray scattering calculations. (a) Asymmetry ratios calculated for a $C = -1$ (left-handed skyrmion). (b) Asymmetry ratios calculated for a $C = +1$ (right-handed) skyrmion. (c) Measured and calculated asymmetry ratios. Experimental data is represented as dots and triangles for $+Q_{\text{lateral}}$ and $-Q_{\text{lateral}}$, respectively. The calculations (lines) are given by an incoherent sum of scattering intensities for two skyrmions with opposite chirality.

There are two possible reasons that the calculated asymmetry at $\pm Q_{\text{lateral}}$ is not antisymmetric. First, since the polarization vector itself is not explicitly included in the resonant scattering amplitude, but is included via the charge quadrupole in the AT form, the scattering may not follow the typical asymmetry rules observed for magnetic structures. In magnetic structures, the chirality and the sign of the asymmetry are likely to be directly related, as is readily observable in existing studies [21–23].

Second, unlike previous x-ray resonant scattering studies on magnetic and nonmagnetic chiral structures, the displacement of the resonant ion itself must be considered in the case of ferroelectric polarization. Since both the AT and ion displacement are involved in the sign of asymmetry, it is not warranted to expect that the sign of the dichroic signal in the wide Q_z region will be reversed simply by reversing the sign of Q_{lateral}.

Furthermore, when comparing the results of Figs. 4(a) and 4(b), which have opposite skyrmion chirality, the asymmetry ratios with opposite signs of satellite peak

order are antisymmetric. For example, the asymmetry ratio for $+Q_{\text{lateral}}$ and chirality $C=-1$ in Fig. 4(a) and the calculated result for $-Q_{\text{lateral}}$ and chirality $C=+1$ in Fig. 4(b) are antisymmetric. This result shows that the sign of the satellite peak is sensitive to the chirality in the polar skyrmions. Because of this, dichroic measurements of resonant scattering such as asymmetry ratio are required to accurately characterize the 3D vector distribution including chirality in the skyrmions.

To understand the experimental asymmetry ratio results of Fig. 3(b), we introduce a simple phenomenological model of the asymmetry ratio $A(Q_z)$. Since the sign of the circular dichroism changes with both the sign of the diffraction order τ and the skyrmion chirality C, the structure factor of the skyrmions $\mathbf{\Psi}$ in Eq. (5) contains terms both with and without the (τ, C) dependence. Considering the x-ray polarization factors in the scattering geometry, which appear effectively as the sign of the diffraction order τ in the dichroic intensities, the asymmetry ratio can be expressed quantitatively as follows:

$$\begin{aligned} A(Q_z) &= \tau[\mathcal{A}(Q_z) + \tau C\mathcal{B}(Q_z)] \\ &= \tau\mathcal{A}(Q_z) + C\mathcal{B}(Q_z), \end{aligned} \tag{6}$$

where $\tau=\pm1$ for $\pm Q_{\text{lateral}}$ and the terms $\mathcal{A}$ and $\mathcal{B}$ do not explicitly include the diffraction order τ or chirality C.

Detailed calculations of $\mathcal{A}$ and $\mathcal{B}$ can be obtained using Eqs. (4), (S3), and (S4). On the other hand, for a one-dimensional polar helix, the analytical formula corresponding to Eq. (6) can be obtained [42]. The terms $\mathcal{A}$ and $\mathcal{B}$ are related to the scattering geometry ($\tau=\pm1$ for $\pm Q_{\text{lateral}}$) and the skyrmion chirality ($C=\pm1$). Now, in the case of $C=-1$ in Fig. 4(a), the asymmetry ratios from Eq. (4) are $\mathcal{A}-\mathcal{B}$ and $-\mathcal{A}-\mathcal{B}$ for $+Q_{\text{lateral}}$ and $-Q_{\text{lateral}}$ satellites, respectively. Similarly, in the case of $C=+1$ in Fig. 4(b), the asymmetry ratios are $\mathcal{A}+\mathcal{B}$ ($+Q_{\text{lateral}}$) and $-\mathcal{A}+\mathcal{B}$ ($-Q_{\text{lateral}}$).

This model accounts for the results of Figs. 4(a) and 4(b) and the fact that the asymmetry ratios of opposite satellites are not antisymmetric for a given skyrmion chirality C. We can also immediately see that the asymmetry ratios of opposite satellites can be antisymmetric to each other (as observed experimentally) when skyrmions with opposite chirality are formed together in one sample. That is, if the skyrmions are mixed in the area from which the scattering event is obtained, the asymmetry ratio at $+Q_{\text{lateral}}$ is $\frac{1}{2}[(\mathcal{A}+\mathcal{B})+(\mathcal{A}-\mathcal{B})]=\mathcal{A}$, and at $-Q_{\text{lateral}}$ is $\frac{1}{2}[(-\mathcal{A}+\mathcal{B})+(-\mathcal{A}-\mathcal{B})]=-\mathcal{A}$, so they are antisymmetric.

The lines in Fig. 4(c) show the calculated asymmetry ratios for the case when skyrmions with opposite chirality [in Figs. 4(a) and 4(b)] have the same coverage and are distributed incoherently. As expected by the phenomenological model in Eq. (5), it is exactly antisymmetric for opposite satellites, so the coexistence of skyrmions with opposite chirality explains the experimental results well. Furthermore, the experimentally observed changes in the sign and magnitude of the asymmetry are reproduced with the model as well. Finally, the antisymmetric feature of the opposite satellites will be immediately broken when the coverage of the opposite chirality skyrmion is biased to either side, so the antisymmetric experimental result is very sensitive to the distribution of the skyrmion chirality. As such, it is clearly shown experimentally that skyrmions with opposite chirality are likely distributed close to 50:50 in our system.

To further investigate the utility of the asymmetry ratio in REXS as a probe of the polar skyrmion structure, we performed calculations to see how changes to the skyrmion structure predicted from second-principles affect the results. As shown in the Supplemental Material [30], moving the center of the skyrmion along the z direction or changing its radial size can have dramatic effects on the magnitude of the predicted asymmetry ratio. This shows not only that the structure from second principles is very close to the real structure, but also that circular dichroism in REXS can probe more than just the handedness of chiral polar structures.

In chiral nanostructures such as polar vortices and skyrmions, being able to identify the handedness is important to understand what affects their chirality, and whether a pure or enantiomorphic mixture forms. In general, it is difficult to determine whether structures of both chiralities exist with a local probe such as scanning transmission electron microscopy (STEM), and it is difficult to measure the 3D distribution of displacement vectors due to the nature of STEM. With four-dimensional STEM, a mixture of right- and left-handed polar vortices has been identified in a single sample [43], but still only two polarization directions can be probed in such a measurement. In contrast, REXS shows that this difficulty can be solved. Since REXS can identify a pure or mixed fraction of right- and left-handed polar skyrmions, this creates opportunities to discover ways to control or switch the chirality of polar nanostructures. For example, the application of an anisotropic strain or an in-plane electric field could potentially couple to the chirality and allow us to switch from one handedness to the other, as has been demonstrated in the polar vortex case [44], which could be readily probed with REXS techniques.

Finally, more complex systems such as multiferroics could benefit from a similar treatment. REXS studies of multiferroic materials are limited, and the interpretation of their results is not trivial because of scattering contributions from multiple order parameters [24]. Because the AT in our framework is completely general, it can capture the effects of charge and magnetic sources of scattering. Applications to nanostructures in multiferroic heterostructures [45] or antiferromagnetic skyrmions [46] could probe their 3D

structure and chirality in a way that has not been achieved previously.

M. R. M. and R. R. were supported by the Quantum Materials program from the Office of Basic Energy Sciences, U.S. Department of Energy (DE-AC02-05CH11231). V. A. S., J. W. F., and L. W. M. acknowledge the U.S. Department of Energy, Office of Science, Office of Basic Energy Sciences, under Award No. DE-SC-0012375 for support to study complex-oxide heterostructure with x-ray scattering. L. W. M. and R. R. acknowledge partial support from the Army Research Office under the ETHOS MURI via cooperative agreement W911NF-21-2-0162. J. Í. acknowledge financial support from the Luxembourg National Research Fund through project FNR/C18/MS/12705883/REFOX. Diamond Light Source, UK, is acknowledged for beam time on beam line I10 under proposal NT24797. K. T. K., S. Y. P., and D. R. L. acknowledge support from the National Research Foundation of Korea, under Grant No. NRF-2020R1A2C1009597, NRF-2019K1A3A7A09033387, and NRF-2021R1C1C1-009494. M. A. P. G. acknowledges support by the Czech Science Foundation (Project No. 19-28594X). This research used resources of the Advanced Light Source, a U.S. DOE Office of Science User Facility under Contract No. DE-AC02-05CH11231. This research used resources of the Advanced Photon Source, a U.S. Department of Energy (DOE) Office of Science User Facility at Argonne National Laboratory and is based on research supported by the U.S. DOE Office of Science-Basic Energy Sciences, under Contract No. DE-AC02-06CH11357. S. D. gratefully acknowledges a start-up grant from Indian Institute of Science, Bangalore, India. F. G.-O., P. G.-F., and J. J. acknowledge financial support from Grant No. PGC2018-096955-B-C41 funded by MCIN/AEI/10.13039/501100011033 and by ERDF "A way of making Europe," by the European Union. F. G.-O. acknowledges financial support from Grant No. FPU18/04661 funded by MCIN/AEI/10.13039/501100011033.

*These authors contributed equally to this work.
†drlee@ssu.ac.kr
‡rramesh@berkeley.edu

[1] X. Zhang, Y. Zhou, K. M. Song, T.-E. Park, J. Xia, M. Ezawa, X. Liu, W. Zhao, G. Zhao, and S. Woo, J. Phys. Condens. Matter **32**, 143001 (2020).
[2] A. Fert, N. Reyren, and V. Cros, Nat. Rev. Mater. **2**, 17031 (2017).
[3] A. Barman, S. Mondal, S. Sahoo, and A. De, J. Appl. Phys. **128**, 170901 (2020).
[4] B. Göbel, I. Mertig, and O. A. Tretiakov, Phys. Rep. **895**, 1 (2021).
[5] N. Nagaosa and Y. Tokura, Nat. Nanotechnol. **8**, 899 (2013).
[6] Y. Tokura and N. Kanazawa, Chem. Rev. **121**, 2857 (2021).
[7] A. K. Yadav, C. T. Nelson, S. L. Hsu, Z. Hong, J. D. Clarkson, C. M. Schlepütz, A. R. Damodaran, P. Shafer, E. Arenholz, L. R. Dedon *et al.*, Nature (London) **530**, 198 (2016).
[8] S. Das, Y. L. Tang, Z. Hong, M. A. P. Gonçalves, M. R. McCarter, C. Klewe, K. X. Nguyen, F. Gómez-Ortiz, P. Shafer, E. Arenholz *et al.*, Nature (London) **568**, 368 (2019).
[9] I. I. Naumov, L. Bellaiche, and H. Fu, Nature (London) **432**, 737 (2004).
[10] I. Naumov and A. M. Bratkovsky, Phys. Rev. Lett. **101**, 107601 (2008).
[11] M. G. Stachiotti and M. Sepliarsky, Ferroelectrics **427**, 41 (2012).
[12] J. Fink, E. Schierle, E. Weschke, and J. Geck, Rep. Prog. Phys. **76**, 056502 (2013).
[13] S. Di Matteo, J. Phys. D **45**, 163001 (2012).
[14] Y. Joly, S. D. Matteo, and O. Bunău, Eur. Phys. J. Special Topics **208**, 21 (2012).
[15] R. Comin and A. Damascelli, Annu. Rev. Condens. Matter Phys. **7**, 369 (2016).
[16] R. J. Green, R. Sutarto, F. He, M. Hepting, D. G. Hawthorn, and G. A. Sawatzky, Synchrotron Radiat. News **33**, 20 (2020).
[17] J. Geissler, E. Goering, M. Justen, F. Weigand, G. Schütz, J. Langer, D. Schmitz, H. Maletta, and R. Mattheis, Phys. Rev. B **65**, 020405(R) (2001).
[18] P. C. Rogge, P. Shafer, G. Fabbris, W. Hu, E. Arenholz, E. Karapetrova, M. P. Dean, R. J. Green, and S. J. May, Adv. Mater. **31**, 1902364 (2019).
[19] H. A. Dürr, E. Dudzik, S. S. Dhesi, J. B. Goedkoop, G. van der Laan, M. Belakhovsky, C. Mocuta, A. Marty, and Y. Samson, Science **284**, 2166 (1999).
[20] W. Legrand, J.-Y. Chauleau, D. Maccariello, N. Reyren, S. Collin, K. Bouzehouane, N. Jaouen, V. Cros, and A. Fert, Sci. Adv. **4**, eaat0415 (2018).
[21] J.-Y. Chauleau, W. Legrand, N. Reyren, D. Maccariello, S. Collin, H. Popescu, K. Bouzehouane, V. Cros, N. Jaouen, and A. Fert, Phys. Rev. Lett. **120**, 037202 (2018).
[22] S. L. Zhang, G. van der Laan, W. W. Wang, A. A. Haghighirad, and T. Hesjedal, Phys. Rev. Lett. **120**, 227202 (2018).
[23] W. Li, I. Bykova, S. Zhang, G. Yu, R. Tomasello, M. Carpentieri, Y. Liu, Y. Guang, J. Gräfe, M. Weigand *et al.*, Adv. Mater. **31**, 1807683 (2019).
[24] J.-Y. Chauleau, T. Chirac, S. Fusil, V. Garcia, W. Akhtar, J. Tranchida, P. Thibaudeau, I. Gross, C. Blouzon, A. Finco *et al.*, Nat. Mater. **19**, 386 (2020).
[25] G. van der Laan, C. R. Phys. **9**, 570 (2008).
[26] Y. Tanaka, T. Kojima, Y. Takata, A. Chainani, S. W. Lovesey, K. S. Knight, T. Takeuchi, M. Oura, Y. Senba, H. Ohashi, and S. Shin, Phys. Rev. B **81**, 144104 (2010).
[27] P. Shafer, P. García-Fernández, P. Aguado-Puente, A. R. Damodaran, A. K. Yadav, C. T. Nelson, S.-L. Hsu, J. C. Wojdeł, J. Íñiguez, L. W. Martin *et al.*, Proc. Natl. Acad. Sci. U.S.A. **115**, 915 (2018).
[28] S. W. Lovesey and G. van der Laan, Phys. Rev. B **98**, 155410 (2018).
[29] G. van der Laan and S. W. Lovesey, Phys. Rev. B **103**, 125124 (2021).
[30] See Supplemental Material at http://link.aps.org/supplemental/10.1103/PhysRevLett.129.247601 for details

about materials growth and experimental methods; S2 for details of the anisotropic tensor calculations; S3 for details on unit cell geometry and anisotropic tensor rotation; S4 for details about calculation of the diffracted intensity; S5 for calculations using modified skyrmion structures; which includes Refs. [31,32].

[31] E. Arenholz, G. van der Laan, A. Fraile-Rodriguez, P. Yu, Q. He, and R. Ramesh, Phys. Rev. B **82**, 140103(R) (2010).

[32] F. M. F. de Groot, J. C. Fuggle, B. T. Thole, and G. A. Sawatzky, Phys. Rev. B **41**, 928 (1990).

[33] G. van der Laan, S. L. Zhang, and T. Hesjedal, AIP Adv. **11**, 015108 (2021).

[34] M. Blume, *Resonant Anomalous X-Ray Scattering*, edited by G. Materlik, C. Sparks, and K. Fisher (North-Holland, Amsterdam, 1994).

[35] J. J. Sakurai, *Advanced Quantum Mechanics* (Addison-Wesley, Redwood City, 1987).

[36] J. P. Hannon, G. T. Trammell, M. Blume, and D. Gibbs, Phys. Rev. Lett. **61**, 1245 (1988).

[37] D. H. Templeton and L. K. Templeton, Acta Cryst. A **38**, 62 (1982).

[38] V. E. Dmitrienko, Acta Crystallogr. Sect. A **39**, 29 (1983).

[39] T. Nagano, J. Kokubun, I. Yazawa, T. Kurasawa, M. Kuribayashi, E. Tsuji, K. Ishida, S. Sasaki, T. Mori, S. Kishimoto, and Y. Murakami, J. Phys. Soc. Jpn. **65**, 3060 (1996).

[40] S. W. Lovesey, E. Balcar, K. Knight, and J. F. Rodríguez, Phys. Rep. **411**, 233 (2005).

[41] K. T. Kim, M. R. McCarter, V. A. Stoica, S. Das, C. Klewe, E. P. Donoway, D. M. Burn, P. Shafer, F. Rodolakis, M. A. Gonçalves *et al.*, Nat. Commun. **13**, 1 (2022).

[42] K. T. Kim, J. Y. Kee, M. R. McCarter, G. van der Laan, V. A. Stoica, J. W. Freeland, R. Ramesh, S. Y. Park, and D. R. Lee, Phys. Rev. B **106**, 035116 (2022).

[43] K. X. Nguyen, Y. Jiang, M. C. Cao, P. Purohit, A. K. Yadav, P. Garca-Fernndez, M. W. Tate, C. S. Chang, P. Aguado-Puente, J. Íñiguez *et al.*, arXiv:2012.04134.

[44] P. Behera, M. A. May, F. Gómez-Ortiz, S. Susarla, S. Das, C. T. Nelson, L. Caretta, S.-L. Hsu, M. R. McCarter, B. H. Savitzky *et al.*, Sci. Adv. **8**, eabj8030 (2022).

[45] A. B. Mei, R. Ramesh, and D. G. Schlom, arXiv:1810.12895.

[46] C. Léveillé, S. Flewett, E. Burgos-Parra, Y. Sassi, W. Legrand, F. Ajejas, V. Cros, N. Reyren, and N. Jaouen, Phys. Rev. B **104**, L060402 (2021).